

Tunable Spatiotemporal Orders in Driven Insulators

Daniel Kaplan,^{1,*} Pavel A. Volkov,^{2,†} Ahana Chakraborty,¹ Zekun Zhuang,³ and Premala Chandra^{1,‡}

¹Center for Materials Theory, Department of Physics and Astronomy,
Rutgers University, Piscataway, NJ 08854, USA

²Department of Physics, University of Connecticut, Storrs, CT 06269, USA

³Department of Physics, University of Wisconsin-Madison, Madison, Wisconsin 53706, USA

We show that driving polar optical phonons above a threshold fluence induces spatiotemporal orders, where polarization or magnetization oscillate at an incommensurate wavevector q_0 in space and at half the drive frequency in time. The order is robust against temperature on timescales much larger than the lifetime of the excited modes and is accompanied by a static $2q_0$ modulation for certain symmetries. We predict its signatures in time-resolved diffraction and provide estimates for candidate materials. Our results open the way to realizing tunable density waves in solids on the nanoscale using THz or IR light.

Introduction— Externally driven condensed matter phases are attracting tremendous interest [1–3] due to the rapid development of ultrafast optics [1–8] and proposals of exotic non-equilibrium phases, such as time crystals [9–14]. In particular, the use of intense terahertz pulses has led to the observation of several light-induced transitions in different quantum materials [1, 7, 8, 15–19]. Recent advances in time-resolved X-ray or electron diffraction, [20, 21], further allow the characterizing of the spatial character of the emergent transient orders on ultrafast time-scales set by the width of the pumping pulse (10^{-12} sec).

The conventional mechanism for such light-driven order involves the light-driven softening of a near-critical mode, resulting in a symmetry-breaking transition [22–29]; this approach is appropriate for materials close to instabilities where accessible fluences are sufficient to affect the ground state. As the nature of the transient order is set by the system’s pre-existing soft modes, its characteristic features are generally not tunable, e.g. in many examples [15–18] the transient order is commensurate with underlying lattice.

In this work, we present an alternative pathway to light-induced phase transitions that results in tunable spatiotemporal orderings due to the interplay of nonlinearity, parametric resonance and spatial dispersion. We consider a resonantly driven polar phonon Q with natural frequency Ω_Q , nonlinearly coupled to another low-energy excitation P , such as a phonon or magnon (Fig. 1 (a,b)). For drive amplitude above a threshold set by the linewidths of Q and P , the modes with energy $\omega_Q/2$ develop a macroscopic expectation value that oscillates in time with frequency $\omega_Q/2$ and space with wavevector q_0 determined by their dispersion (Fig. 1 (c)). Our numerical results indicate that the resulting spatiotemporal order is generally stable against temperature, and we predict its signatures in time-resolved diffraction experiments on candidate materials.

Model and Equations of Motion— The key features for inducing spatiotemporal order are shown in Fig. 1(c): optical ($Q_i(r, t)$) and vector ($P_i(r, t)$) (either polar or axial)

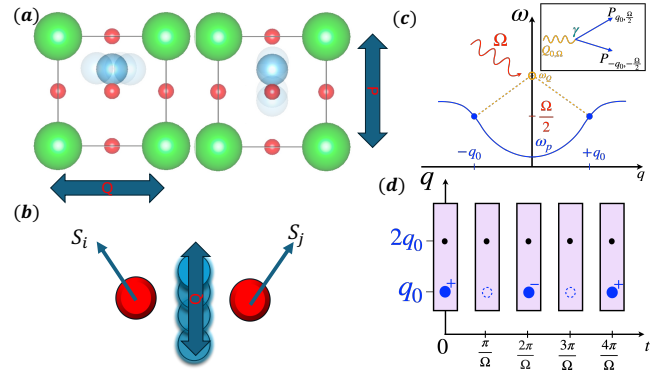


Figure 1. Schematic of the dynamical ordering mechanism. (a) In a ferroelectric, substantial nonlinear coupling is expected between an optical phonon mode Q and a lower energy mode P , that displaces the same ion. These describe the amplitude and orientational excitations of the ferroelectric order. (b) In inversion symmetric systems, the excitation of an optical polar phonon of a non-magnetic ion Q can drive a dynamical DM interaction, of magnetic moments S_i, S_j . (c) Spatiotemporal orderings result from parametric resonance: resonant pumping of the Q mode at frequency Ω excites a finite momentum P mode at $\Omega/2$ via nonlinear interaction (inset). (d) Diffraction signatures of the resulting dynamical and static orders. The blue dots denote the relative intensity of the Bragg peak at q_0 measured at time intervals of π/Ω . The second feature at $2q_0$ is time-independent and significantly weaker.

modes with frequencies ω_Q and ω_P respectively such that $\omega_P < \omega_Q$ and, close to Γ , $\omega_P^2(q) = \omega_P^2(0) + v_P^2 q^2$ is the dispersion for P . Q is resonantly pumped so that $\Omega \approx \omega_Q$. Even neglecting the small wavevector of the driving electromagnetic waves, nonlinear parametric resonance generates a macroscopic expectation values of the P mode at frequency $\Omega/2$ and wavevector q_0 which is determined by its dispersion $\omega_P(q_0) = \Omega/2$. The effect is driven by a cubic coupling as shown in the inset of Fig. 1(c). As discussed below, at finite wavevector a coupling of this type can be present for any symmetry group. Furthermore, a cubic nonlinearity of the P mode, if allowed, results in a static modulation at $2q_0$. Two kinds of Bragg peaks are

then expected in time-resolved diffraction experiments [21, 30–33]: one at q_0 whose amplitude varies frequency $\frac{\Omega}{2}$ and a second weaker static one at $2q_0$ (Fig. 1(d)). We model the nonlinear interaction between the two modes and the driving of Q with the potential,

$$V_{\text{int}}(Q, P) = Z\vec{Q} \cdot \vec{E}(t) + z_1\vec{Q} \cdot \vec{P} + \xi_{ijk}Q_iP_jP_k + \xi'_{ijk}Q_iQ_jP_k + \delta_{ijkl}(Q_iP_j)\partial_kP_l + \dots \quad (1)$$

And allow for nonlinearities in the modes via,

$$V_{\text{nl}}(Q, P) = \alpha_Q Q^3 + \alpha'_Q Q^4 + \alpha_P P^3 + \alpha'_P P^4. \quad (2)$$

We begin with a concrete example of two coupled polar phonons in a ferroelectric (Fig. 1 (a)). In particular, we take the Q mode to be the amplitude mode of the ferroelectric order, while the P mode corresponds to the fluctuations of the ion orthogonal to the polarization. The lowest order nonlinear terms in energy density can be obtained from Landau theory (see SM), result in $z_1 = \xi' = 0$. We also set $\delta_{ijkl} = 0$ as this term is subleading in a ferroelectric system. Its effect is examined in the Discussion. We note that cubic self-interaction such as α_P is allowed only if the corresponding mirror symmetry is broken as is the case in rhombohedral BaTiO₃ or monoclinic CaTiO₃. Assuming a symmetry group where $\xi_{ijk} = \gamma$, the classical equations of motion are,

$$\ddot{Q} - v_Q^2 \nabla^2 Q + \omega_Q^2 Q + \beta \dot{Q} = E(t) - \gamma P^2 - \frac{\partial V_{\text{nl}}(Q)}{\partial Q} + \eta(r, t), \quad (3)$$

$$\ddot{P} - v_P^2 \nabla^2 P + \omega_P^2 P + \beta \dot{P} = -2\gamma PQ - \frac{\partial V_{\text{nl}}(P)}{\partial P} + \eta(r, t). \quad (4)$$

where dissipation and temperature are modeled with isotropic damping ($\beta\dot{Q}, \beta\dot{P}$) and Langevin, $\eta(r, t)$ terms respectively. We consider 1D solutions, $P = P(x, t)$ and $Q = Q(x, t)$, and orient both fields along the polar axis.

Numerical Solutions at $T = 0$.— We solve (3)-(4) numerically, drawing $P(x, 0), Q(x, 0)$ from a uniform distribution with a small amplitude (where $|P(x_i, 0)| < \frac{1}{N_x}$, where N_x is the discretization along the x axis) and zero initial velocities \dot{Q}, \dot{P} such that all terms in V_{nl} are negligible. Eqs. (3)-(4) are solved using standard methods for Langevin dynamics [34], satisfying the CFL criterion [35] for all parameters thus guaranteeing stability of the numerical integration. For fields $E < E_c$, we find that for any set of initial conditions the P mode decays exponentially on a scale of $1/\beta$; a representative solution is presented in Fig. 2(a). Nonetheless, the observed dynamics contains information about the coupling between the modes and the dispersion. In particular, the structure factor $S(q, \omega) = \int dx dt P(x, t) e^{iqx} e^{i\omega t}$; $\ln|S(q, \omega)|$ (Fig. 2(d)) shows a pronounced branch in frequency-momentum

space reflecting the dispersion of the P mode. For $E > E_c$, a regular pattern emerges at late times (Fig. 2(b)), oscillating in time with frequency $\Omega/2$. This ($q_0, \frac{\Omega}{2}$) order also has a fingerprint in $S(q, \omega)$ (Fig. 2(e)), where an extremely strong peak at $q_0 \approx 3.1/(2\pi a)$ appears (note the logarithmic scale different from scale Fig. 2(d)). A partial structure factor analysis, $S(q, t \rightarrow \infty)$, for $E < E_c$ and $E > E_c$ is plotted in Fig. 2(f), indicating a delta-like peak for $E > E_c$ at $q = |q_0|$. The initial-condition averaged value of $P_{q_0, \Omega/2}$ as a function of field amplitude is presented in Fig. 2(c). The onset of a finite $|P_{q_0, \Omega/2}|$ above E_c is continuous and follows $\sim \sqrt{E - E_c}$.

Next we introduce a non-negligible cubic nonlinearity for the P mode in V_{nl} and plot the resulting spectral function in Fig. 3(a); comparison with Fig. 2(e) indicates a new static ($\omega = 0$) feature at $2q_0$ whose amplitude is weaker than that of $|P_{q, \Omega/2}|$. In Fig. 3(b) the scaling of this mode $|P_{2q_0, 0}|$ as a function of fluence is displayed; $|P_{2q_0, 0}| \sim (E - E_c)$, indicating a continuous transition at the same E_c as $|P_{q_0, \frac{\Omega}{2}}|$ but with a higher exponent.

Nonlinear Parametric Resonance— Inspired by the numerical results, we show that the tunable spatiotemporal order results from parametric resonance [36] at finite momentum. We approximate the the fields Q, P by the contributions of three modes that dominate to the dynamics at $E > E_c$: $Q(x, t) \propto Q_{0, \Omega} e^{i\Omega t} + c.c.$ and $P(x, t) \approx P_{q_0, \Omega/2} e^{i(\frac{\Omega}{2}t - q_0x)} + P_{q_0, -\Omega/2} e^{-i(\frac{\Omega}{2}t + q_0x)} + c.c..$ Using this ansatz, the equations for the mode amplitudes are

$$\Omega^2 Q_{0, \Omega} - \omega_Q^2 Q_{0, \Omega} - i\Omega\beta Q_{0, \Omega} = -E_0/2 + 2\gamma P_{q_0, \Omega/2} P_{q_0, -\Omega/2}^* \quad (5)$$

$$(\Omega/2)^2 P_{q_0, \Omega/2} - (\omega_P^2 + v_P^2 q_0^2) P_{q_0, \Omega/2} - i(\Omega/2)\beta P_{q_0, \Omega/2} = 2\gamma Q_{0, \Omega} P_{q_0, -\Omega/2} \quad (6)$$

We take the resonant limit ($\Omega \rightarrow \omega_Q$) and consider P modes satisfying the parametric resonance condition, which is set by the momentum q_0 for which $\delta\omega_P^2 = (\Omega/2)^2 - (\omega_P^2 + v_P^2 q^2)$ vanishes identically. Equations (5)-(6) now become

$$-i\Omega\beta Q_{0, \Omega} = -E_0/2 + 2\gamma P_{q_0, \Omega/2} P_{q_0, -\Omega/2}^* \quad (7)$$

$$i\beta\Omega/2 P_{q_0, \Omega/2} = 2\gamma Q_{0, \Omega} P_{q_0, -\Omega/2}. \quad (8)$$

The equations for $P_{\pm q_0, -\Omega/2}$ differ by $\Omega \rightarrow -\Omega, Q_{0, \Omega} \rightarrow Q_{0, \Omega}^*$ in (8), implying that $|P_{q_0, \Omega/2}| = |P_{q_0, -\Omega/2}|$. This allows to introduce $P_{q_0, \pm\Omega/2} = |P_{q_0, \Omega/2}| e^{i\varphi \pm \Omega t}$. Solving Eq. (8) for $Q_{0, \Omega}$ and substituting the result in (7), we get an equation on $P_{q_0, \pm\Omega/2}$: $e^{i(\varphi\Omega - \varphi - \Omega)} [\beta^2 \Omega^2 / 4\gamma + 2\gamma |P_{q_0, \Omega/2}|^2] = E_0/2$. A solution exists for $E_0 > E_c$, where $\varphi_\Omega = \varphi - \Omega$ and

$$E_0 \geq \frac{\beta^2 \Omega^2}{2\gamma}, \quad |P_{q_0, \Omega/2}| = \frac{1}{2\sqrt{\gamma}} \sqrt{E_0 - \beta^2 \Omega^2 / (2\gamma)}. \quad (9)$$

indicating that this spatiotemporal ordering onsets in a continuous transition in excellent agreement with our

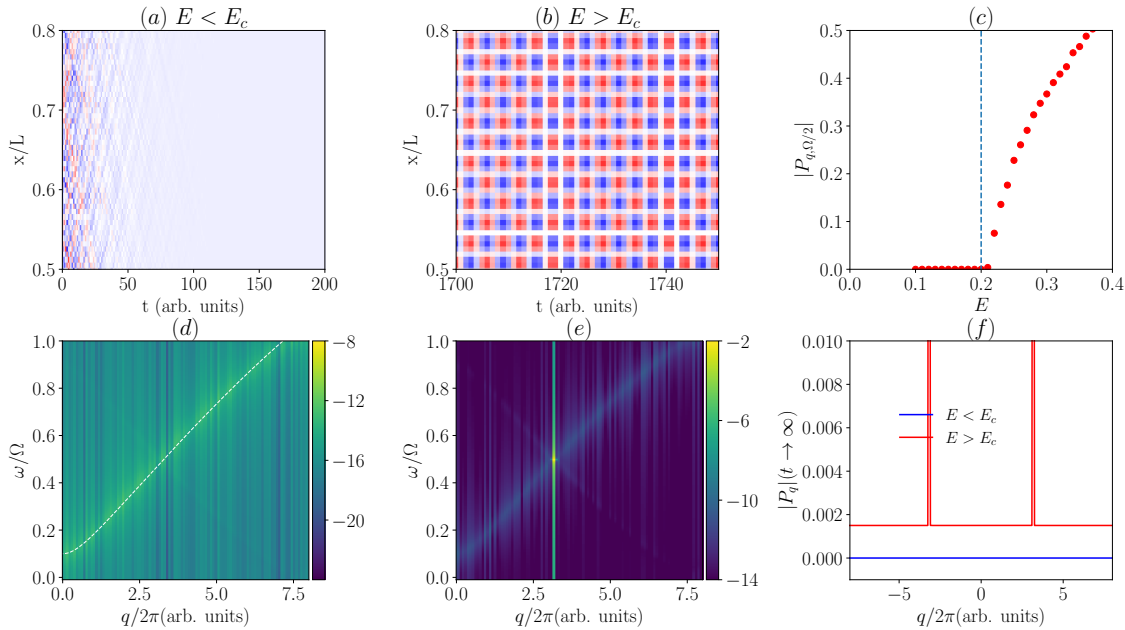


Figure 2. General solution of the coupled nonlinear equations at $T = 0$. (a) Spatial distribution of the mode $P(x, t)$ for electric field strength E below the threshold E_c . (b) Symmetry-broken phase shown for $E > E_c$, zooming in on x/L and $t \gg 1/\beta$ (within the steady state); P oscillates in both space and time signifying spatio-temporal order. This order is stable on all scales for times greater than $1/\beta$. (c) Amplitude of the parametrically excited mode $P_{q, \Omega/2}$ as a function of E . For the parameters selected here, $P_{q, \Omega/2}$ appears at $E \approx 0.2$. The blue dashed line indicated the critical value calculated from Eq. (9). The vanishing of $P_{q, \Omega/2}$ is continuous. (d) Log of the spectral function $\ln|S(q, \omega)|$ (see main text). For clarity, the dispersion of $P(x, t)$ is superimposed with a dashed white line. For $E < E_c$, the amplitude is exponentially suppressed, but signatures of the bare band structure of $P(x, t)$ are visible. (e) $\ln|S(q, \omega)|$ for $E > E_c$, showing the sharp peak at $q \approx 3.1$ and $\omega = \Omega/2$ confirming the parametric resonance. (f) Fourier transform of $P(x, t)$ in q at late times. Clearly visible $q \approx 3.1$ peak appears only for $E > E_c$. Parameters used here are: $\omega_P = 0.2$, $\Omega = \omega_Q = 2.0$, $\beta = 0.1$, $v_P = 4 \cdot 10^{-3}$, $\gamma = 0.1$, $\alpha'_{Q,P} = 0.0001$.

numerics (Fig. 2(c)); the order parameter $|P_{q_0, \Omega/2}|$ vanishes below a critical value of E_0 that depends on the dissipation β and the nonlinear coupling γ . Note that the individual phases $\varphi_{\pm\Omega/2}$ of $P_{q_0, \pm\Omega/2}$ are undetermined by the above equations, indicating that any value can be realized depending on initial conditions, in agreement with our numerical results. This suggests a spontaneously broken spatial translation symmetry of the steady state. We include a separate discussion on detuned driving in the SM.

Static Spatial Order— Nonlinear self-interaction terms in V_{nl} produce additional static modulated ordering, and here we focus on the leading term in V_{nl} , $\alpha_P P^3$. For a finite value of $|P_{q_0, \frac{\Omega}{2}}|$, this cubic coupling acts as a source in the time-independent version of Eq. 4 which becomes $-v_P^2 \partial_x^2 P = -2\gamma PQ - 3\alpha P^2$. A solution is obtained iteratively: Fourier transforming and assuming P_{2q_0} is small, we have $4v_P^2 q_0^2 P_{2q_0} = -3\alpha P_{q_0, \Omega/2} P_{q_0, -\Omega/2}$. The QP term is neglected as it does not contain Fourier components at $2q_0$ to leading order. The solution is then $|P_{2q_0}| = \frac{3\alpha |P_{q_0, \Omega/2}|^2}{4v_P^2 q_0^2}$. This allows for the prediction that

whereas $|P_{q, \Omega/2}| \sim \sqrt{E - E_c}$, $|P_{2q, \Omega}| \sim |E - E_c|$, in agreement with our numerics (Fig. 3(b)).

Finite-Temperature Numerical Results— Above we have shown that the steady state is characterized by a spontaneously broken translation symmetry characterized by a phase φ . In order to assess the stability of this state, we now include temperature modeled as a noise term in our numerical simulations. We find that the phase of φ remains unaffected until T is comparable to this mode's classical energy due to driving. In Fig. 4(a), we show the real-space image of the excited state. For T comparable to the energy at the bottom of P band, $T \sim \omega_P^2 \langle P^2 \rangle$ (where this scale sets the energy of a classical oscillator), the phase remains nearly fixed in time over many cycles of the external drive Ω . When the temperature to meet the scales set by $\omega_P^2 = (\omega_P^2(0) + v_P^2 q_0^2) \langle P^2 \rangle$, significant fluctuations in phase occur and order is ultimately suppressed. At intermediate scales (orange curve in Fig. 4(c)), the phase exhibits a nearly linear drift, suggesting that it carries out a diffusive random walk as expected for thermal effects. For a generic equilibrium system, such a random walk of the phase is expected to destroy long-range spatial

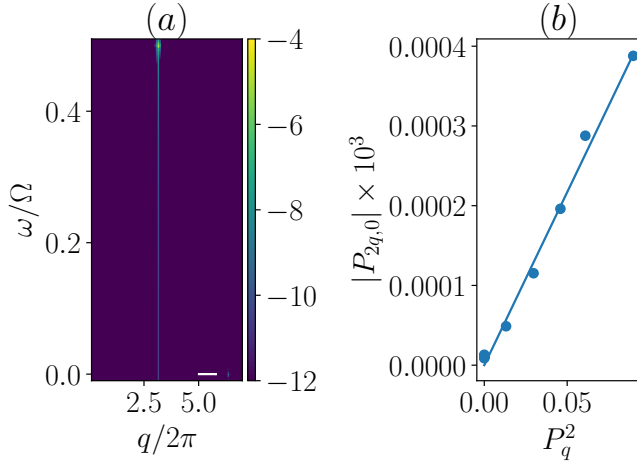


Figure 3. Finite $2q, \omega = 0$ modulation with additional nonlinearity at $T = 0$. (a) Spectral function focusing on the segment with $q > 3$ and $\omega < 1/2\Omega$. Note the additional peak at $2q \approx 6.2/(2\pi a)$, see peak next to the white bar. The peak at $q \approx 3.1/(2\pi a)$ is unchanged. This mode is static in time. (b) Dependence of the amplitude of the $P_{2q, \omega=0}$ mode as a function of P_q . Note that $P_{2q} \propto |P_q|^2$ plotted in Fig. 2(c). Parameters identical with Fig. 2(c), but with $\alpha_P = 0.01$.

order following the Hohenberg-Mermin-Wagner theorem [37, 38]. Surprisingly, here the phase remains relatively stable for more than $\sim 10^3$ cycles for a wide range of T below the classical energy of the mode. The stability of the spatiotemporal order here has been confirmed numerically for a wide range of initial conditions and realizations. The significant suppression of fluctuations may be attributed to nonlinearities in P , as has been observed for models of flocking where nonlinearities stabilize order out of equilibrium [39, 40]. However, our present results can not rule out an alternative scenario, where the system will eventually thermalize after an emergent long prethermalization time [10, 12]. We leave a detailed investigation of late-time dynamics to future work. As most current experiments on materials are performed with relatively short pump times, rather than continuous pumping, the stability of the order at finite time scales that we demonstrate should be sufficient for the experimental detection of spatiotemporal order.

Generalizations and Material Platforms— Although the results we presented here focused on 1D dispersion of the coupled P, Q modes, they can be easily generalized to the 2D and 3D cases. There, a whole manifold of \vec{q} set by $|\delta\omega_P(\vec{q})| = 0$ would be parametrically excited, though we expect only a discrete number of symmetry-related \vec{q} will yield the lowest threshold fluence. Similar behavior has been observed in ultracold atomic Bose-Einstein condensates [41]. Furthermore, of the remaining discrete set of \mathbf{q} points, nonlinearities in the fields will select stable configurations with lower symmetries in the steady state. Increased dimensionality may also further

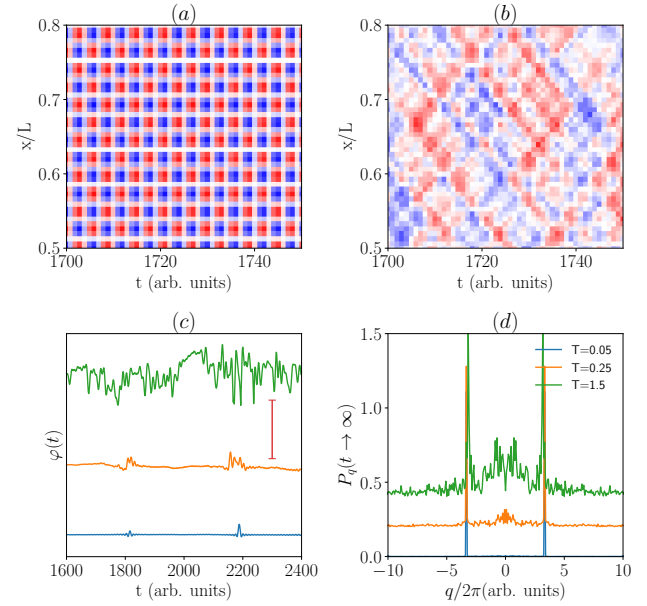


Figure 4. General solution at finite temperature $T \neq 0$. (a) Ordered, fixed phase solution at low temperature, $T = 0.05 \sim \omega_P^2(0)\langle P^2 \rangle$. (b) Substantial phase variation in the solution. Here $T \sim \omega_P^2(q_0)\langle P^2 \rangle$, that is, at the scale of the classical energy of the parametrically excited modes (see main text). (c) Phase of the mode φ as a function of t for $\sim 10^3$ cycles of the drive. For $T = 0.05$, the phase is nearly perfectly constant in time. For intermediate temperature, e.g. $T = 0.25$, a gradual drift is observed. For temperature on the scale of $\omega_P^2(q_0)\langle P^2 \rangle$ significant phase fluctuations are observed. Red scale bar measures deviation of $\pi/2$. (d) Momentum decomposition of the condensed mode P_q at long times at three temperatures, denoting the low, intermediate and high energy scales (see main text). For all temperatures, the effect allows for thermal occupation of low energy modes, leading to a Gaussian spreading of the weight for all momenta.

stabilize the system against thermal fluctuations.

The mechanism explored here for ferroelectrics can be straightforwardly applied to a number of systems, the key ingredient being the cubic nonlinearity between two modes, QP^2 . For polar materials, such a coupling is allowed to P mode of any symmetry, including magnetic ones, provided that Q is a polar phonon along the order parameter. In the SM, we show that the coupling can be generically large if the P, Q originate from the same ion; in this scenario, $\gamma \sim \delta Q/Q_0$, where Q_0 is the ferroelectric order parameter and δQ is the drive-induced modulation. This is also depicted in Fig. 1 (a). For a general case, we have estimated E_c for PbTiO_3 taking E phonon at $\approx 275\text{cm}^{-1}$ [42] as Q , another E phonon at $\approx 90\text{cm}^{-1}$ as P . Using parameters in Ref. [23]; we estimate $E_0 \approx 3.55\text{MV/cm}$ and $q_0 \approx 0.95\text{\AA}^{-1}$, realistic for potential experiments.

Our proposal does not require polar order or inversion symmetry breaking; cubic coupling to the polar mode

can be achieved in materials with inversion symmetry via gradient coupling $\delta_{ijkl}Q_iP_j\nabla_kP_l$, $\delta_{ijkl} \neq 0$. For a “frozen” Q , such couplings are known as Lifshitz invariants [43] and can be constructed for structural [44], incommensurate [45], magnetic [46, 47] and even superconducting [48, 49] orders.

The magnetic case corresponds to the Dzyaloshinskii-Moriya interaction [46, 47] with a dynamical DM vector set by the polar phonon displacement. This idea may open an alternative path for localized magnon generation (due to large q_0) in the THz regime, allowing for faster nanoscale magnonic computation [50]. Intriguingly, the intensely studied NiO, has TO phonons [51] at about 30 – 40 meV, while the magnon band extends from few to 100 meV [52], opening the path to the creation of spatiotemporal order with THz magnons. Another potential application of our proposal is in accessing magnon dispersion in 2D materials, such as CrI₃, where magnons close to the K point are predicted to possess a topological gap [53].

Finally, parametric phenomena have a long history in physics [36] and continue to be explored in a variety of systems [10, 12, 54]. The key novelty of our proposal is to use nonlinear phononics to induce strong parametric phenomena in solids. For magnetic materials, a qualitative advantage of the mechanism proposed in this work is that the excitation occurs by electric field, allowing for a much stronger impact on the material than magnetic field, typically used. So far, electric field driving of magnons has been achieved only in synthetic systems with lower frequency scales [55, 56]. For phononic materials, on the other hand, our proposal may allow to realize tunable dynamic superlattices.

Discussion and Conclusions— In this work we have presented a mechanism for spatiotemporal ordering in solids using a nonlinear parametric resonance created by a driven optical phonon. Since a uniform electric field cannot generally transfer momentum to an excitation in a solid, the mechanism presented here is a direct way of generating tunable finite momentum order with light. With additional nonlinearities in the excited field P , it is possible to produce static order which spatially oscillates at twice the momentum $2q_0$ of the parametrically excited mode. We make specific predictions for Bragg diffraction measurements in candidate materials involving both polarization and magnetization spatiotemporal orderings.

The driven spatiotemporal orders presented here can be further used to address challenges in other fields: e.g. to generate nanometer-wavelength THz- and IR-frequency magnons [50] or superlattices with the static $2q_0$ components for the other degrees of freedom, allowing to create tunable periodic potentials with short wavelength $1/2q_0$, beyond the possibilities of lithographic techniques.

Acknowledgements. We thank B. L. Altshuler, S. L. Sondhi, R. Moessner, Anirvan Sangupta, Andrea Cavalleri and Benoit Fauque for inspiring discussions. D. Kaplan is supported by the Abrahams Postdoctoral Fellowship

of the Center for Materials Theory, Rutgers University and the Zuckerman STEM Fellowship. This research was supported in part by grant NSF PHY-2309135 to the Kavli Institute for Theoretical Physics (KITP) [PAV]. PAV acknowledges support by the University of Connecticut OVPR Quantum CT seed grant.

* d.kaplan1@rutgers.edu

† pavel.volkov@uconn.edu

‡ premla@physics.rutgers.edu

- [1] D. Basov, R. Averitt, and D. Hsieh, Towards properties on demand in quantum materials, *Nature materials* **16**, 1077 (2017).
- [2] A. de la Torre, D. M. Kennes, M. Claassen, S. Gerber, J. W. McIver, and M. A. Sentef, Colloquium: Nonthermal pathways to ultrafast control in quantum materials, *Reviews of Modern Physics* **93**, 041002 (2021).
- [3] J. Bloch, A. Cavalleri, V. Galitskii, M. Hafezi, and A. Rubio, Strongly correlated electron-photon systems, *Nature* **606**, 41 (2022).
- [4] J. Hebling, K.-L. Yeh, M. C. Hoffmann, B. Bartal, and K. A. Nelson, Generation of high-power terahertz pulses by tilted-pulse-front excitation and their application possibilities, *JOSA B* **25**, B6 (2008).
- [5] P. Emma, R. Akre, J. Arthur, R. Bionta, C. Bostedt, J. Bozek, A. Brachmann, P. Bucksbaum, R. Coffee, F.-J. Decker, et al., First lasing and operation of an ångström-wavelength free-electron laser, *nature photonics* **4**, 641 (2010).
- [6] M. Buzzi, M. Först, R. Mankowsky, and A. Cavalleri, Probing dynamics in quantum materials with femtosecond x-rays, *Nature Reviews Materials* **3**, 299 (2018).
- [7] A. Disa, T. Nova, and A. Cavalleri, Engineering crystal structures with light, *Nature Physics* **17**, 1087 (2021).
- [8] M. Henstridge, M. Först, E. Rowe, M. Fechner, and A. Cavalleri, Nonlocal nonlinear phonics, *Nature Physics* **18**, 457 (2022).
- [9] V. Khemani, R. Moessner, and S. L. Sondhi, A brief history of time crystals, arXiv:1910.10745 (2019).
- [10] M. P. Zaletel, M. Lukin, C. Monroe, C. Nayak, F. Wilczek, and N. Y. Yao, Colloquium: Quantum and classical discrete time crystals, *Rev. Mod. Phys.* **95**, 031001 (2023).
- [11] A. Shapere and F. Wilczek, Classical time crystals, *Phys. Rev. Lett.* **109**, 160402 (2012).
- [12] N. Y. Yao, C. Nayak, L. Balents, and M. P. Zaletel, Classical Discrete Time Crystals, *Nature Physics* **16**, 438 (2020).
- [13] F. Wilczek, Quantum time crystals, *Phys. Rev. Lett.* **109**, 160401 (2012).
- [14] V. Khemani, A. Lazarides, R. Moessner, and S. L. Sondhi, Phase structure of driven quantum systems, *Phys. Rev. Lett.* **116**, 250401 (2016).
- [15] T. Nova, A. Disa, M. Fechner, and A. Cavalleri, Metastable ferroelectricity in optically strained strontium titanate, *Science* **364**, 1075 (2019).
- [16] X. Li, T. Qiu, J. Zhang, E. Baldini, J. Lu, A. M. Rappe, and K. A. Nelson, Terahertz field-induced ferroelectricity in quantum paraelectric *SrTiO₃*, *Science* **364**, 1079 (2019a).

- [17] X. Li, T. Qiu, J. Zhang, E. Baldini, J. Lu, A. M. Rappe, and K. A. Nelson, Terahertz field-induced ferroelectricity in quantum paraelectric SrTiO_3 , *Science* **364**, 1079 (2019b).
- [18] A. Disa, J. Curtis, M. Fechner, A. Liu, A. Von Hoegen, M. Först, T. Nova, P. Narang, A. Maljuk, A. Boris, et al., Photo-induced high-temperature ferromagnetism in YTiO_3 , *Nature* **617**, 73 (2023).
- [19] B. Cheng, P. L. Kramer, Z.-X. Shen, and M. C. Hoffmann, Terahertz-driven local dipolar correlation in a quantum paraelectric, *Physical Review Letters* **130**, 126902 (2023).
- [20] M. Fechner, M. Först, G. Orenstein, V. Krapivin, A. S. Disa, M. Buzzi, A. von Hoegen, G. de la Pena, Q. L. Nguyen, R. Mankowsky, M. Sander, H. Lemke, Y. Deng, M. Trigo, and A. Cavalleri, Quenched lattice fluctuations in optically driven SrTiO_3 , *Nature Materials* **23**, 363 (2024), arXiv:2301.08703 [cond-mat.mtrl-sci].
- [21] G. Orenstein, V. Krapivin, Y. Huang, Z. Zhang, G. de la Pena Munoz, R. Duncan, Q. Nguyen, J. Stanton, S. Teitelbaum, H. Yavas, T. Sato, M. Hoffman, P. Kramer, J. Zhang, A. Cavalleri, R. Comin, M. Dean, A. Disa, M. Först, S. Johnson, M. Mittrano, A. Rappe, D. Reis, D. Zhu, K. Nelson, and M. Trigo, Observation of Polarization Density Waves in SrTiO_3 , arXiv:2403.17203 (2024).
- [22] A. Subedi, A. Cavalleri, and A. Georges, Theory of nonlinear phononics for coherent light control of solids, *Phys. Rev. B* **89**, 220301 (2014).
- [23] A. Subedi, Proposal for ultrafast switching of ferroelectrics using midinfrared pulses, *Phys. Rev. B* **92**, 214303 (2015).
- [24] A. Subedi, Midinfrared-light-induced ferroelectricity in oxide paraelectrics via nonlinear phononics, *Phys. Rev. B* **95**, 134113 (2017).
- [25] M. Puviani and M. A. Sentef, Quantum nonlinear phononics route towards nonequilibrium materials engineering: Melting dynamics of a ferroelectric charge density wave, *Phys. Rev. B* **98**, 165138 (2018).
- [26] P. G. Radaelli, Breaking symmetry with light: Ultrafast ferroelectricity and magnetism from three-phonon coupling, *Phys. Rev. B* **97**, 085145 (2018).
- [27] D. Shin, S. Latini, C. Schäfer, S. A. Sato, E. Baldini, U. De Giovannini, H. Hübener, and A. Rubio, Simulating terahertz field-induced ferroelectricity in quantum paraelectric SrTiO_3 , *Physical Review Letters* **129**, 167401 (2022).
- [28] Z. Zhuang, A. Chakraborty, P. Chandra, P. Coleman, and P. A. Volkov, Light-driven transitions in quantum paraelectrics, *Phys. Rev. B* **107**, 224307 (2023).
- [29] D. Kuzmanovski, J. Schmidt, N. A. Spaldin, H. M. Rønnow, G. Aeppli, and A. V. Balatsky, Kapitza stabilization of quantum critical order, *Phys. Rev. X* **14**, 021016 (2024).
- [30] G. A. de la Peña Muñoz, A. A. Correa, S. Yang, O. Delaire, Y. Huang, A. S. Johnson, T. Katayama, V. Krapivin, E. Pastor, D. A. Reis, et al., Ultrafast lattice disordering can be accelerated by electronic collisional forces, *Nature Physics* **19**, 1489 (2023).
- [31] Y. Huang, P. Sun, S. W. Teitelbaum, H. Li, Y. Sun, N. Wang, S. Song, T. Sato, M. Chollet, T. Osaka, I. Inoue, R. A. Duncan, H. D. Shin, J. Haber, J. Zhou, M. Bernardi, M. Gu, J. M. Rondinelli, M. Trigo, M. Yabashi, A. A. Maznev, K. A. Nelson, D. Zhu, and D. A. Reis, Hard x-ray generation and detection of nanometer-scale localized coherent acoustic wave packets in SrTiO_3 and KTaO_3 (2024), arXiv:2312.16453 [cond-mat.mtrl-sci].
- [32] B. Fauqué, P. Bourges, A. Subedi, K. Behnia, B. Baptiste, B. Roessli, T. Fennell, S. Raymond, and P. Steffens, Mesoscopic fluctuating domains in strontium titanate, *Phys. Rev. B* **106**, L140301 (2022).
- [33] A. S. Johnson, D. Perez-Salinas, K. M. Siddiqui, S. Kim, S. Choi, K. Volckaert, P. E. Majchrzak, S. Ulstrup, N. Agarwal, K. Hallman, et al., Ultrafast x-ray imaging of the light-induced phase transition in VO_2 , *Nature Physics* **19**, 215 (2023).
- [34] B. Leimkuhler and C. Matthews, Robust and efficient configurational molecular sampling via langevin dynamics, *The Journal of chemical physics* **138** (2013).
- [35] P. D. Lax, Stability of difference schemes, *The Courant–Friedrichs–Lewy (CFL) Condition: 80 Years After Its Discovery*, 1 (2013).
- [36] L. Landau and E. Lifshitz, *Mechanics* (Pergamon Press, 1976).
- [37] N. D. Mermin and H. Wagner, Absence of ferromagnetism or antiferromagnetism in one- or two-dimensional isotropic heisenberg models, *Phys. Rev. Lett.* **17**, 1133 (1966).
- [38] B. Halperin, On the hohenberg-mermin-wagner theorem and its limitations, *J. Stat. Phys.* **175**, 521 (2019).
- [39] J. Toner and Y. Tu, Long-range order in a two-dimensional dynamical XY model: How birds fly together, *Phys. Rev. Lett.* **75**, 4326 (1995).
- [40] J. Toner, Y. Tu, and S. Ramaswamy, Hydrodynamics and phases of flocks, *Ann. Phys.* **318**, 170 (2005).
- [41] M. Bukov, S. Gopalakrishnan, M. Knap, and E. Demler, Prethermal floquet steady states and instabilities in the periodically driven, weakly interacting bose-hubbard model, *Phys. Rev. Lett.* **115**, 205301 (2015).
- [42] N. Choudhury, E. J. Walter, A. I. Kolesnikov, and C.-K. Loong, Large phonon band gap in SrTiO_3 and the vibrational signatures of ferroelectricity in $a\text{Tio}_3$ perovskites: First-principles lattice dynamics and inelastic neutron scattering, *Phys. Rev. B* **77**, 134111 (2008).
- [43] L. D. Landau and E. M. Lifshitz, *Statistical Physics: Volume 5*, Vol. 5 (Elsevier, 2013).
- [44] H. T. Stokes, D. M. Hatch, and H. M. Nelson, Landau, lifshitz, and weak lifshitz conditions in the landau theory of phase transitions in solids, *Phys. Rev. B* **47**, 9080 (1993).
- [45] V. Kopsky and D. G. Sannikov, Gradient invariants and incommensurate phase transitions, *Journal of Physics C: Solid State Physics* **10**, 4347 (1977).
- [46] T. Moriya, Anisotropic superexchange interaction and weak ferromagnetism, *Physical review* **120**, 91 (1960).
- [47] I. Dzyaloshinsky, A thermodynamic theory of “weak” ferromagnetism of antiferromagnetics, *Journal of physics and chemistry of solids* **4**, 241 (1958).
- [48] V. P. Mineev and K. V. Samokhin, Nonuniform states in noncentrosymmetric superconductors: Derivation of lifshitz invariants from microscopic theory, *Phys. Rev. B* **78**, 144503 (2008).
- [49] R. Nagashima, S. Tian, R. Haenel, N. Tsuji, and D. Manske, Classification of lifshitz invariant in multiband superconductors: An application to leggett modes in the linear response regime in kagome lattice models, *Phys. Rev. Res.* **6**, 013120 (2024).
- [50] A. Barman, G. Gubbiotti, S. Ladak, A. O. Adeyeye, M. Krawczyk, J. Gräfe, C. Adelman, S. Cotofana, A. Naemi, V. I. Vasyuchka, B. Hillebrands, S. A. Nikitov,

- H. Yu, D. Grundler, A. V. Sadovnikov, A. A. Grachev, S. E. Sheshukova, J.-Y. Duquesne, M. Marangolo, G. Csaba, W. Porod, V. E. Demidov, S. Urazhdin, S. O. Demokritov, E. Albisetti, D. Petti, R. Bertacco, H. Schultheiss, V. V. Kruglyak, V. D. Poimanov, S. Sahoo, J. Sinha, H. Yang, M. Münzenberg, T. Moriyama, S. Mizukami, P. Landeros, R. A. Gallardo, G. Carlotti, J.-V. Kim, R. L. Stamps, R. E. Camley, B. Rana, Y. Otani, W. Yu, T. Yu, G. E. W. Bauer, C. Back, G. S. Uhrig, O. V. Dobrovolskiy, B. Budinska, H. Qin, S. van Dijken, A. V. Chumak, A. Khitun, D. E. Nikonov, I. A. Young, B. W. Zingsem, and M. Winklhofer, The 2021 magnonics roadmap, *Journal of Physics: Condensed Matter* **33**, 413001 (2021).
- [51] A. Floris, S. de Gironcoli, E. K. U. Gross, and M. Cococcioni, Vibrational properties of mno and nio from dft + u -based density functional perturbation theory, *Phys. Rev. B* **84**, 161102 (2011).
- [52] M. T. Hutchings and E. J. Samuelsen, Measurement of spin-wave dispersion in nio by inelastic neutron scattering and its relation to magnetic properties, *Phys. Rev. B* **6**, 3447 (1972).
- [53] A. T. Costa, D. L. R. Santos, N. M. Peres, and J. Fernández-Rossier, Topological magnons in cri3 monolayers: an itinerant fermion description, *2D Materials* **7**, 045031 (2020).
- [54] R. Kleiner, Z. Zhou, E. Dorsch, X. Zhang, D. Koelle, and D. Jin, Space-Time Crystalline Order of a High-Critical Temperature Superconductor with Intrinsic Josephson Junctions, *Nature Communications* **12**, 6038 (2021).
- [55] R. Verba, V. Tiberkevich, I. Krivorotov, and A. Slavin, Parametric excitation of spin waves by voltage-controlled magnetic anisotropy, *Phys. Rev. Appl.* **1**, 044006 (2014).
- [56] Y.-J. Chen, H. K. Lee, R. Verba, J. A. Katine, I. Barsukov, V. Tiberkevich, J. Q. Xiao, A. N. Slavin, and I. N. Krivorotov, Parametric resonance of magnetization excited by electric field, *Nano letters* **17**, 572 (2017).